A Practical Circuit-based Model for Li-ion Battery Cells in Electric Vehicle Applications

Long Lam, Pavol Bauer
Department of Electrical Sustainable Energy
Delft University of Technology
Delft, the Netherlands
P.Bauer@tudelft.nl

Erik Kelder
Department of Chemical Engineering
Delft University of Technology
Delft, the Netherlands
E.M.Kelder@tudelft.nl

Abstract—**This paper proposes a practical circuit-based model for Li-ion cells, which can be directly connected to a model of a complete electric vehicle (EV) system. The goal of this paper is to provide EV system designers with a tool in simulation programs such as Matlab/Simulink to model the behaviour of Li-ion cells under various operating conditions in EV or other applications. The current direction, state of charge (SoC), temperature and C-rate dependency are represented by empirical equations obtained from measurements on $LiFePO_4$ cells. Tradeoffs between model complexity and accuracy have been made based on practical considerations in EV applications. Depending on the required accuracy and operating conditions, the EV system designer can choose the influences to be included in the system simulation.**

Keywords: **$LiFePO_4$, battery model, regenerative braking, electric vehicle, practical circuit model.**

I. INTRODUCTION

Batteries, instead of the engine, have become the heart of the car in the transition from internal combustion engine (ICE) vehicles to electric vehicles (EVs). In designing EVs it is therefore important to be able to simulate the behaviour of the battery system, in particular the battery pack. Hence, a battery model that can be directly connected to a model of the rest of the electronic system is required.

In the field of battery modelling many different battery models have been proposed in literature [1]. The battery models can be divided into analytical, electrochemical and electrical circuit models or a combination of the model types. Analytical models [2] do not give a good view of the electrochemical processes occurring in the cell. Electrochemical models [3][4] require a large amount of computational power to solve the time-varying spatial partial differential equations and cannot be directly connected to the rest of the system. Combined analytical and electrochemical models [5][6] also suffer from high complexity and poor system modelling compatibility. On the other hand, electrical circuit models can easily be connected to the rest of the electronic systems, but suffer from lower accuracy [7][8]. Nevertheless, to model the general behaviour of the battery in an EV system electrical circuit models are sufficient.

Most electrical circuit models can be classified as impedance-based [9][10] or Thevenin-based [11][12] models. Impedance-based models require Electrochemical Impedance Spectroscopy (EIS) to determine the circuit components; the circuit components are related to electrochemical processes in the cell. In Thevenin-based models the circuit component values are extracted from the measured voltage response. The advantage of Thevenin-based models is that using various algorithms [13][14] the circuit components can be extracted from voltage measurements of an operating EV battery without any additional equipment in the EV.

The equivalent circuit-based model developed by Chen & Rincón-Mora [15] is capable of modelling the runtime, DC, AC and transient response of a single cell. Other works have attempted to include the C-rate effect [16], temperature effect and capacity fading [17] in the capacity of the cell using the model in [15]. However, only the discharge phase of the cell has been modelled and regenerative braking has not been considered. Chan & Sutanto [18] recognised the need to model the charging phase of the cell in EV applications, and introduced separate circuit components for discharging and charging. The model was expanded with additional circuit components for modelling in circuit simulation programs, but suffered from incapability to model fast transitions between discharging and charging states [19]. In Matlab/Simulink the model can, however, be implemented by nonlinear equations for each circuit components [20], removing the need for separate circuit components for discharging and charging.

In this paper a practical electrical circuit model based on [15] for EVs will be proposed. The model consists of empirical equations extracted from measurements on $LiFePO_4$ cells. With adjustments to the equations and parameters other battery chemistries can also be modelled. The goal of the model is to provide EV system designers with a tool to simulate the behaviour of $LiFePO_4$ cells under possible operating conditions in simulation programs such as Matlab/Simulink, and not to validate the characteristics of the cells. The focus of this paper will lie on the short term behaviour of the cell, but the long term behaviour will be touched upon. Empirical equations are presented to model the influence of different temperatures and C-rates on the discharging and charging behaviour of the cells. In contrast to previous works of other authors, an attempt will be made to relate the different influences on the electrochemical processes to the correct circuit components instead of the cell capacity. This utilises EV system designers to simulate the energy efficiency of a cell as well.

978-1-4577-1250-0/11/$26.00 ©2011 IEEE

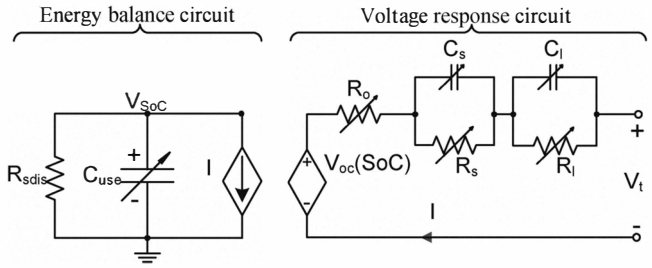

Fig. 1. The proposed model based on [15].

This paper is organised as follows. Section II presents the proposed model. The extraction of the empirical equations and parameters for the proposed model is described in section III. In section IV the proposed model is validated by comparing the simulation results with the measurements. Section V concludes this paper.

II. PROPOSED MODEL

Fig. 1 shows the battery cell model proposed in this work. The circuit is divided into an energy balance and voltage response circuit. Each circuit component is made variable, since they depend on various factors such as temperature, C-rate (capacity normalised current) and state of charge (SoC). The energy balance circuit models the cell capacity with C_{use} and the self-discharge with R_{sdis}. V_{SoC} is circuit representation of SoC and the value is equal to SoC. Therefore only SoC will be used in this paper. The voltage response circuit consists of the open-circuit voltage (OCV) V_{oc}, the ohmic resistance R_o, the short time transient parallel RC pair R_s and C_s, and the long time transient parallel RC pair R_l and C_l. With the OCV and the internal cell impedance the voltage response of the cell is modelled under different operating conditions.

In the model the useable capacity C_{use} is the current independent capacity of the cell; this is the theoretically possible amount of charge that can be discharged from a fully charged cell with an infinitely small current for a given minimum cell voltage, so that the voltage drop over the internal resistance becomes close to zero. Furthermore, the SoC used in the model is thermodynamic-SoC (t-SoC) in contrast to the often used engineering-SoC (e-SoC) [21]. The e-SoC is the state of the cell capacity apparent to the user and is current dependent. The t-SoC is the SoC defined by the thermodynamic properties in the cell and is directly related to the OCV of the cell, i.e. the state of the useable capacity. Since the current effect on the capacity is already taken into account by the internal impedance, it would be duplication to model the energy balance circuit with the apparent capacity and e-SoC.

In the practical equivalent circuit-based model it is not important if every influence on the cell has been taken into account, but whether the different influences have a noticeable effect on the behaviour of the cell. Each impedance element in the voltage response circuit can be related to electrochemical processes in the cell by comparing the circuit with an impedance-based model. Impedance-based models characterise the internal cell impedance obtained from EIS measurements with a 2nd order Randles circuit shown in Fig. 2. R_b is the bulk resistance of the cell, accounting for the electric conductivity of the electrolyte, separator and electrodes. R_{SEI} and C_{SEI} represent the resistance and capacitance of the surface film layer on the

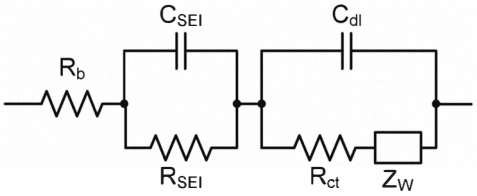

Fig. 2. A typical 2nd order Randles circuit used in impedance-based models.

electrodes e.g. the solid electrolyte interface (SEI) layer and corresponds to the high frequency impedances [9]. The charge transfer resistance R_{ct} and double layer capacitance C_{dl} characterise the activation polarisation voltage drop and the Warburg impedance Z_W represents the diffusion of the lithium ions in the cell. In real-life EV applications the data sample rate is limited and can be as low as 1 Hz, causing the high frequency impedance R_{SEI} and C_{SEI} to be indiscernible from R_b. Furthermore, Z_W can be approximated by a number of parallel RC pairs in series with the rest of the circuit [22] to represent the diffusion phenomena in the cell. Consequently, the electrochemical processes modelled in the impedance-based model are related to the proposed model as following: the ohmic resistance R_o consists of the bulk resistance and surface layer impedance, the activation polarisation is modelled by R_s and C_s, and the concentration polarisation as a result of low diffusion rate is represented R_l and C_l.

In the practical equivalent circuit-based model R_{sdis} is considered to be infinite, since $LiFePO_4$ cells have a very low self-discharge [23]. The OCV has been reported to exhibit a hysteresis effect [11][24] and temperature dependency [20]. Temperature and C-rate dependence have also been reported for the impedance elements [25], although the Li-ion chemistry was not $LiFePO_4$. Equations of various complexities have been proposed to describe the circuit components in literature [15][20]. From measurements it has to be determined which level of complexity is required to reach sufficient accuracy and which influences have to be taken into account in the practical equivalent circuit-based model for $LiFePO_4$ cells.

III. EMPIRICAL MODELLING

Numerous experiments have been conducted on $LiFePO_4$ cells to determine various influences on the circuit components in the proposed model. Empirical equations describing the influences were then extracted from the measurements.

A. Experimental setup

A123 Systems' APR18650m1 $LiFePO_4$ cells of 1.1Ah nominal capacity obtained from a third party vendor have been used in the experiment with a Maccor Series 2000 Automated Battery tester. The battery tester has 16 independent channels with a maximum rating of 10V and 2A. The data was logged on the internal memory of the battery tester and occasionally written to the PC. The cells were placed in closed temperature regulated chambers and initially the surface temperature change of each cell was monitored. However, the temperature change was very small during testing and the cell temperature was assumed to be equal to the temperature of the chamber.

B. Measurement method

The values for the circuit components in the proposed model were extracted with a similar method as described in

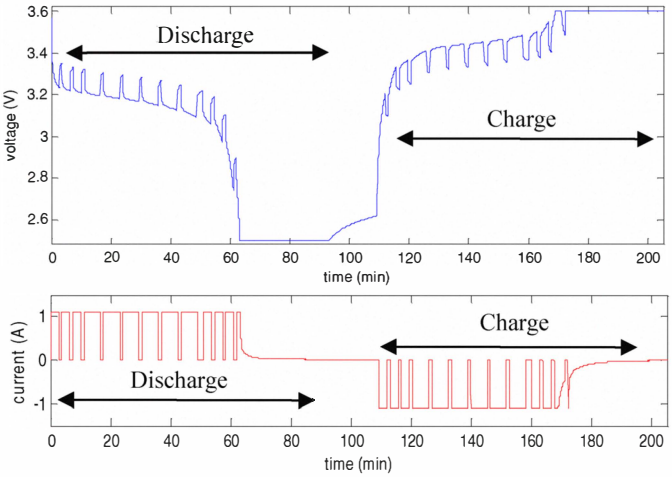

Fig. 3. The test cycle for determining the capacity and parameter of the equivalent circuit components of a cell under test.

[26]. Each cell was charged with the constant current constant voltage (CCCV) method. The cells were charged with the recommended current up to 3.6V, and then charged at constant voltage until the current was lower than 0.01C. The cells were then rested for at least an hour before experiments were conducted. Cells for modelling the temperature influence on the circuit components were rested for at least 6 hours at the test temperature for the cells to reach thermal equilibrium.

The values of the circuit components have been determined by the test cycle shown in Fig. 3. In the nonlinear voltage region cells were discharged with 1C in steps of 0.05Ah and rested for 1 minute. In the linear voltage region cells were discharged with 1C in 0.1Ah steps before rested for 1 minute until the cell had been fully discharged. To approximate the useable capacity of the cell, cells were both charged and discharged with the CCCV method. The minimum cell voltage was set to 2.5V to prevent overdischarge. After a resting period of 15 minutes, the same sequence was repeated for charging. From experiments with different resting times it has been determined the designated resting times were sufficient to have a negligible influence on the practical model.

C. *Useable capacity modelling*

Changes in the useable capacity C_{use} can be either a result of irreversible capacity loss or reversible capacity change. The irreversible capacity loss is known as capacity fading and is a result of cell ageing due to cycling or storage. Capacity fading depends on many stress factors such as temperature, C-rate, SoC and depth of discharge. The reversible capacity change is only dependent on temperature and is generally modelled with the Arrhenius equation. By plotting the natural logarithm of the capacity against 1000/T in Fig. 4a it was, however, found that the capacity development did not satisfy the Arrhenius equation. The natural logarithm of the capacity changed with a curve, which suggested that the Vogel-Tammann-Fulcher (VTF) equation could model the reversible capacity change as shown in Fig. 4b. With the VTF equation the equation for the useable cell capacity was found to be

$$C_{use} = (Q_{nom} - \xi) \cdot e^{k_1\left(\frac{1}{T-k_2} - \frac{1}{T_{ref}-k_2}\right)}, \qquad (1)$$

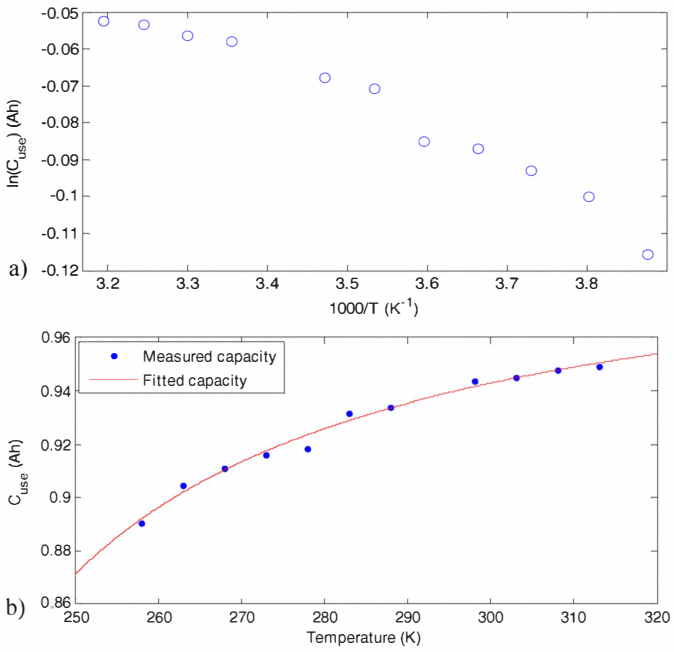

Fig. 4. a) The natural logarithm of the capacity vs. 1000/T and (b) the measured temperature dependency of the capacity with the corresponding curve fit according to the VTF equation.

where Q_{nom} is the initial capacity in Ah and ξ the amount of capacity faded in Ah, both determined at reference temperature T_{ref}. The measured temperature T and T_{ref} are in Kelvin. The parameters k_1 and k_2 are given in Table I.

D. *Open-circuit voltage modelling*

The OCV was determined with the same test procedure as in Fig. 3, but with two hours rest instead of one min to measure the close-to-equilibrium open-circuit voltage (cte-OCV) for discharging and charging. Furthermore, each resting period occurred after every 5% SoC instead of every 0.05Ah or 0.1Ah. The cte-OCV for discharging and charging were averaged to obtain the OCV as shown in Fig. 5. Possible hysteresis of the OCV was neglected, as this is modelled by the internal cell impedance. The OCV was strongly dependent on the SoC and by curve fitting the data in Fig. 5 an equation modelling the OCV was obtained as

$$V_{oc}(SoC) = a_1 e^{-a_2 SoC} + a_3 + a_4 SoC + a_5\, e^{\frac{a_6}{1-SoC}}. \qquad (2)$$

The values for the parameters a_1 to a_6 are given in Table I. OCV measurements have been conducted at temperatures from -20°C to 40°C to determine the temperature dependence of the OCV. The deviations from reference temperature were found to be less than 2mV at most temperatures, going up to 8mV at -20°C. Since the temperature fluctuations were insignificantly small, the OCV is considered temperature independent.

TABLE I. PARAMETER VALUES FOR C_{USE} AND V_{OC}

k_1	-5.738	a_3	3.414
k_2	2.099E2	a_4	1.102E-1
a_1	-5.863E-1	a_5	-1.718E-1
a_2	21.90	a_6	8.000E-3

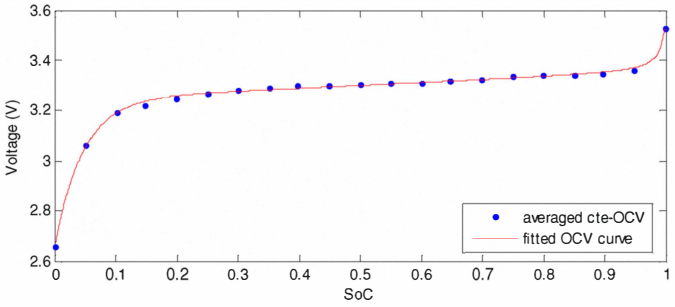

Fig. 5. The averaged cte-OCV measurement and the corresponding OCV model.

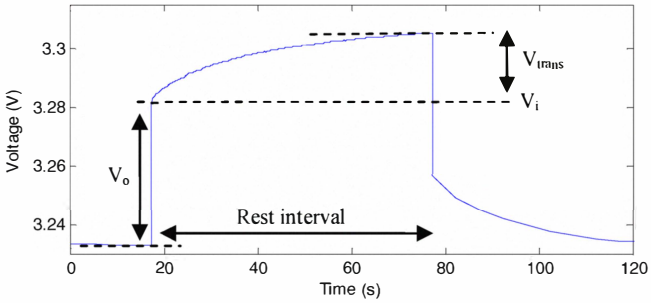

Fig. 6. An example of the voltage response during a rest interval of a discharge test cycle.

E. *Internal impedance modelling*

The internal impedance elements were determined from the voltage response during the rest period as described in [27]. In the practical equivalent circuit-based model the voltage drop within one second is considered to be the instantaneous voltage drop U_o. The short-time and long-time transient parallel RC pairs are determined by curve fitting the rest of the voltage response to the following equations:

$$V_{trans} = V_s\left(1 - e^{-\frac{t}{\tau_s}}\right) + V_l\left(1 - e^{-\frac{t}{\tau_l}}\right) \quad (3)$$

$$V_s = R_s I \quad (4)$$

$$V_l = R_l I = \left(\frac{(V_{oc} - V_i)}{I} - R_s\right) I \quad (5)$$

$$\tau_s = R_s C_s \qquad \tau_l = R_l C_l. \quad (6)$$

V_{trans} is the voltage response minus V_o, V_s and V_l respectively the short and long time transient voltage drop with the time constants τ_s and τ_l , V_{oc} the OCV at the measured SoC and V_i the voltage after the instantaneous voltage drop as shown in Fig. 6. I is the current in Amps before the rest interval, positive for discharging and negative for charging. The resistances and time constants are determined by curve fitting with the nonlinear least squares method in Matlab. The short time transient time constant is determined to be several seconds, and the rest of the voltage response until the OCV is contributed by the long time transient voltage drop.

From the measurements it was determined that the impedance elements for discharging were not equal to charging, resulting in two sets of equations per impedance element. It was found that only between 70% and 40% SoC the voltage response can be approximated with the same equations for discharge and charge. In Fig. 7 and Fig. 8 the values of the impedance elements determined for respectively discharging and charging at 1C are shown to be dependent on the SoC. Using empirical equations consisting of exponential functions and polynomials, the SoC dependence was modelled with the tradeoff between accuracy and complexity of the equations in mind. For discharging the equations of the impedance elements are given by

$$R_{od}(SoC) = b_{1d}SoC^4 + b_{2d}SoC^3 + b_{3d}SoC^2 + b_{4d}SoC + b_{5d} \quad (7)$$

$$R_{sd}(SoC) = c_{1d}e^{-c_{2d}SoC} + c_{3d} + c_{4d}SoC \quad (8)$$

$$C_{sd}(SoC) = d_{1d}SoC^3 + d_{2d}SoC^2 + d_{3d}SoC + d_4 \quad (9)$$

$$R_{ld}(SoC) = g_{1d}e^{-g_{2d}SoC} + g_{3d} + g_{4d}SoC \quad (10)$$

$$C_{ld}(SoC) = h_{1d}SoC^6 + h_{2d}SoC^5 + h_{3d}SoC^4 + h_{4d}SoC^3 + h_{5d}SoC^2 + h_{6d}SoC + h_{7d}. \quad (11)$$

The values of the discharge parameters are given in Table II. The subscript d represents the discharging impedance and parameters of the impedance elements. The equations of the impedance elements for charging are labelled with a subscript c and are given by

$$R_{oc}(SoC) = b_{1c}SoC^4 + b_{2c}SoC^3 + b_{3c}SoC^2 + b_{4c}SoC + b_{5c} \quad (12)$$

$$R_{sc}(SoC) = c_{1c}e^{-c_{2c}SoC} + c_{3c} \quad (13)$$

$$C_{sc}(SoC) = d_{1c}SoC^4 + d_{2c}SoC^3 + d_{3c}SoC^2 + d_{4c}SoC + d_{5c} \quad (14)$$

$$R_{lc}(SoC) = g_{1c}e^{-g_{2c}SoC} + g_{3c} + g_{4c}SoC \quad (15)$$

$$C_{lc}(SoC) = h_{1c}SoC^5 + h_{2c}SoC^4 + h_{3c}SoC^3 + h_{4c}SoC^2 + h_{5c}SoC + h_{6c}. \quad (16)$$

In Table III the values of the charge parameters are given. The equations for discharging and charging are depicted in respectively Fig. 7 and Fig. 8. As a result of curve fitting, C_{sc} and C_{lc} are negative near 100% SoC. The negative value is prevented by implementing a minimum value in the simulation for C_{sc} and C_{lc}. The validity of the equations has been confirmed by determining the SoC dependence of numerous cells of the same type and manufacturer. Each cell shows the same SoC dependence modelled by equations 7 to 16.

TABLE II. IMPEDANCE PARAMETERS FOR DISCHARGING

b_{1d}	1.298E-1	c_{4d}	-6.462E-3	g_{4d}	-2.420E-2
b_{2d}	-2.892E-1	d_{1d}	1.697E2	h_{1d}	2.130E6
b_{3d}	2.273E-1	d_{2d}	-1.007E3	h_{2d}	-6.007E6
b_{4d}	-7.216E-2	d_{3d}	1.408E3	h_{3d}	6.271E6
b_{5d}	8.980E-2	d_{4d}	3.897E2	h_{4d}	-2.958E6
c_{1d}	1.080E-2	g_{1d}	2.950E-1	h_{5d}	5.998E5
c_{2d}	11.03	g_{2d}	20.00	h_{6d}	-3.102E4
c_{3d}	1.827E-2	g_{3d}	4.722E-2	h_{7d}	2.232E3

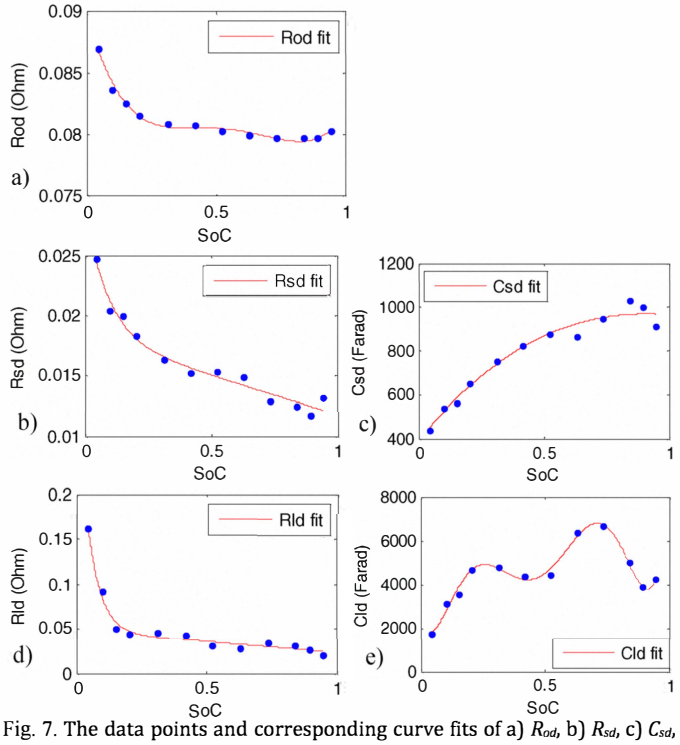

Fig. 7. The data points and corresponding curve fits of a) R_{od}, b) R_{sd}, c) C_{sd}, d) R_{ld} and e) C_{ld} for discharge.

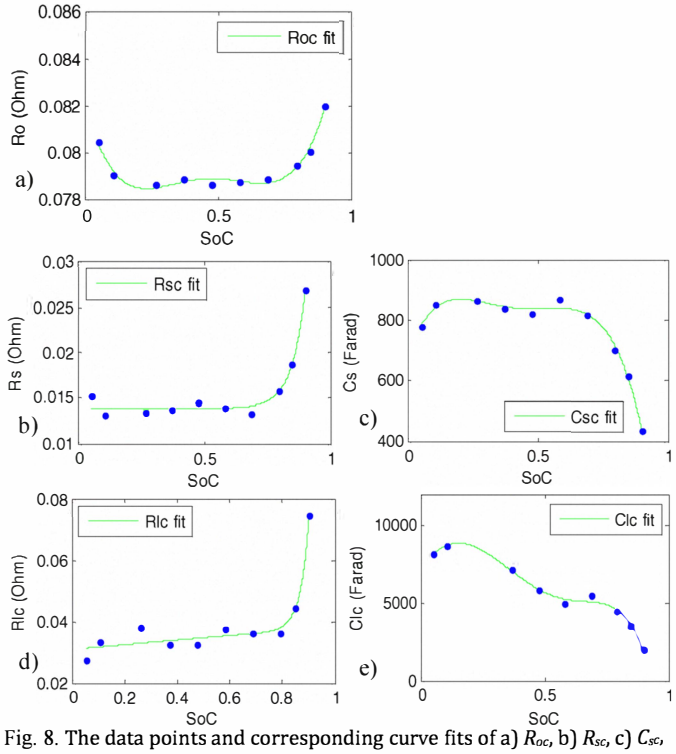

Fig. 8. The data points and corresponding curve fits of a) R_{oc}, b) R_{sc}, c) C_{sc}, d) R_{lc} and e) C_{lc} for charge.

To test the temperature dependence of the impedance elements, the temperature of one cell was varied from 40°C to -15°C in steps of 5°C. At each temperature the impedance elements were determined at 1C as shown in Fig. 9 for discharging. The impedance elements for charging showed a similar behaviour. It can clearly be seen that the SoC behaviour of the impedance elements changes with temperature and can therefore not be regarded as temperature independent. Furthermore, the SoC behaviour changes between 25°C and 15°C. To limit the complexity of the equations, the temperature dependence modelling is split into equations for 20°C and above (high temperatures) and below 20°C (low temperatures). Since the impedance equations were obtained from curve fitting the voltage response, the impedance elements do not directly represent electrochemical processes in a cell, but can only be related to the processes. Consequently, equations describing the temperature dependence of the electrochemical processes cannot be used with the model and the temperature dependence has to be modelled with empirical equations as well. For high temperatures equations 7 to 11 then become

$$R_{od,T_{high}}(SoC,T) = R_{od}(SoC)\cdot b_{t1d}e^{\frac{b_{t2d}}{T-b_{t3d}}} \quad (17)$$

$$R_{sd,T_{high}}(SoC,T) = R_{sd}(SoC) + c_{t1d}\Delta T + c_{t2d}\Delta T\cdot SoC \quad (18)$$

$$C_{sd,T_{high}}(SoC,T) = C_{sd}(SoC) + d_{t1d}\Delta T\cdot SoC + d_{t2d}\Delta T \quad (19)$$

$$R_{ld,T_{high}}(SoC,T) = R_{ld}(SoC) + (g_{t1d}\Delta T)e^{-g_{2d}SoC} + g_{t2d}\Delta T \quad (20)$$

$$C_{ld,T_{high}}(SoC,T) = C_{ld}(SoC)\cdot h_{t1d}e^{\frac{h_{t2d}}{T}}, \quad (21)$$

TABLE III. IMPEDANCE PARAMETERS FOR CHARGING

b_{1c}	1.369E-1	d_{1c}	-1.026E4	g_{4c}	7.473E-3
b_{2c}	-2.518E-1	d_{2c}	1.723E4	h_{1c}	-1.541E5
b_{3c}	1.609E-1	d_{3c}	-1.013E4	h_{2c}	2.042E5
b_{4c}	-4.100E-2	d_{4c}	2.340E3	h_{3c}	-4.009E3
b_{5c}	8.210E-2	d_{5c}	6.849E2	h_{4c}	-8.124E4
c_{1c}	5.896E-10	g_{1c}	8.913E-15	h_{5c}	2.283E4
c_{2c}	-18.75	g_{2c}	-32.23	h_{6c}	7.144E3
c_{3c}	1.388E-2	g_{3c}	3.100E-2		

where T is the temperature in Kelvin and ΔT the temperature deviation from the reference temperature. The parameters with a subscript t are additional parameters introduced to model the temperature dependence and are given in Table IV For high temperatures the impedance model for charging modelled with equations 12 to 16 change to:

$$R_{oc,T_{high}}(SoC,T) = R_{oc}(SoC)\cdot b_{t1c}e^{\frac{b_{t2c}}{T-b_{t3c}}} \quad (22)$$

$$R_{sc,T_{high}}(SoC,T) = c_{t1c}e^{c_{t2c}T-(c_{t3c}T+c_{t4c})SoC} + c_{t5c}T + c_{t6c} \quad (23)$$

$$C_{sc,T_{high}}(SoC,T) = C_{sc}(SoC) + d_{t1c}\Delta T \quad (24)$$

$$R_{lc,T_{high}}(SoC,T) = R_{lc}(SoC)\cdot(g_{t1c}T + g_{t2c}) \quad (25)$$

$$C_{lc,T_{high}}(SoC,T) = C_{lc}(SoC)\cdot h_{t1c}e^{h_{t2c}T}. \quad (26)$$

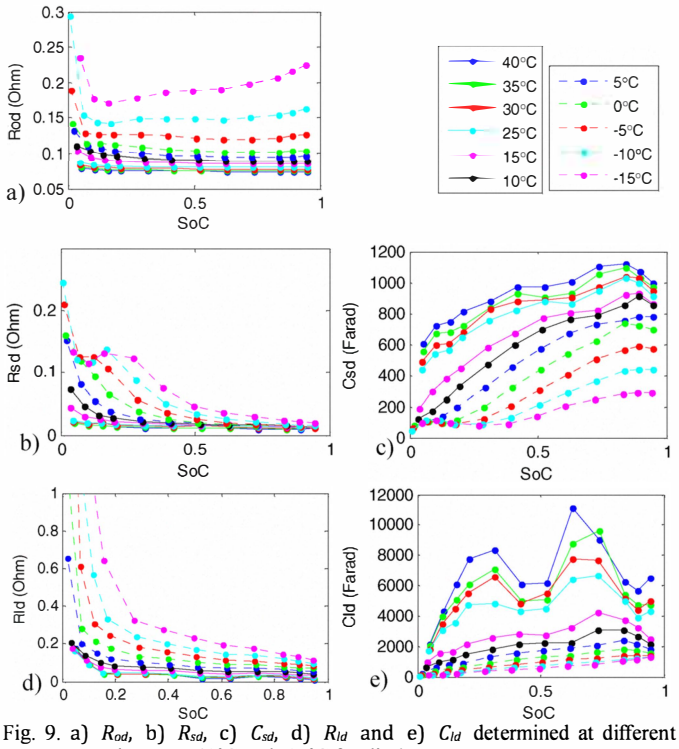

Fig. 9. a) R_{od}, b) R_{sd}, c) C_{sd}, d) R_{ld} and e) C_{ld} determined at different temperatures between 40°C and -15°C for discharge.

Only the equation of R_{sc} is completely changed to model the temperature dependence for high temperatures. The parameters for the temperature dependence are given in Table V. For low temperatures the equations in the impedance model become much more complex as the SoC behaviour changes dramatically. The impedance element equations for low temperatures are given in the Appendix.

The C-rate dependence of the impedance elements was determined by conducting the test cycle at different C-rates between 1.75C and 0.25C with steps of 0.25 at reference temperature. For both discharging and charging the impedance elements were almost invariant with the C-rate except for R_l. This is also reflected in the value of the total resistance R_{tot} for both discharge and charge, which C-rate dependent variations correspond with R_l as shown in Fig. 10. By including the C-rate dependency equations 20 and 25 will respectively become

$$R_{ld,T_{high}}(SoC,T,I) = R_{ld,T_{high}}(SoC,T) \cdot (g_{i1d} {I_{Crate}}^{g_{i2d}} + g_{id3}) \quad (27)$$

$$R_{lc,T_{high}}(SoC,T,I) = R_{lc,T_{high}}(SoC,T) \cdot (g_{i1c}({I_{Crate}}^{g_{i2c}} - 1)SoC + {I_{Crate}}^{g_{i3c}}), \quad (28)$$

where I_{Crate} is the current of the cell in C-rates. The parameters with a subscript i model the C-rate dependency and are given in Table VI. For low temperatures the C-rate dependence can be modelled in the same way.

The C-rate dependence has only been validated for reference temperature and the correlation with the temperature dependence needs further investigation. Additionally, the C-rate dependency modelling of R_{ld} and R_{lc} has a limitation. Equations 27 and 28 are not valid when no current flows in the cell, so when the cell is at rest. R_{ld} and R_{lc} will then take on the values before the cell was in rest. However, due to the switching time of the power electronics, the current is not directly cut-off, but gradually reduces to zero. In that case R_{ld} and R_{lc} will be modelled with the current before the current switch-off occurred. In practical EV applications this will most likely not be a problem as the sampling times are larger than the converter switching times. So to model and predict the general short term behaviour of a cell under possible operating conditions, the proposed practical equivalent circuit-based model is sufficient.

TABLE IV. IMPEDANCE PARAMETERS FOR DISCHARGING AT HIGH TEMPERATURES

b_{t1d}	7.613E-1	c_{t2d}	2.225E-4	g_{t2d}	-5.967E-4
b_{t2d}	10.14	d_{t1d}	-6.580	h_{t1d}	3.128E3
b_{t3d}	2.608E2	d_{t2d}	12.11	h_{t2d}	-2.398E3
c_{t1d}	-3.697E-4	g_{t1d}	6.718E-3		

TABLE V. IMPEDANCE PARAMETERS FOR CHARGING AT HIGH TEMPERATURES

b_{t1c}	7.192E-1	c_{t3c}	-1.178E-1	g_{t1c}	-1.344E-2
b_{t2c}	33.91	c_{t4c}	13.99	g_{t2c}	5.011
b_{t3c}	1.999E2	c_{t5c}	-1.897E-4	h_{t1c}	2.611E-5
c_{t1c}	9.869E8	c_{t6c}	7.054E-2	h_{t2c}	3.541E-2
c_{t2c}	-1.479E-1	d_{t1c}	8.814		

Finally, the long term behaviour of the internal cell impedance has also been investigated. Over the course of an extensive cycling experiment for capacity fading determination, the change in the internal cell impedance has also been measured. The results of the capacity fading experiment will be described in another paper. Only R_o was found to vary during cycling. Furthermore, the change in R_o was constant over the entire SoC region and equal in magnitude for discharging and charging. Consequently, the resistance rise due to ageing can be modelled by solely R_o with the same equation for discharging and charging. However, no pattern was observed in the R_o development during the cycling experiment. A possible explanation is that the runtime of the cycling experiment was insufficient to observe any change. Another possibility is the influence of the current profile used for cycling. The cells in the capacity fading experiment were continuously cycled with a current profile containing regenerative braking and only resting times at the end and beginning of each cycle. Under this cycling profile the resistance growth in the cell may not have been stable, leading to fluctuations in R_o. On the other hand, cells cycled without regenerative braking did show a rising trend of R_o. The ageing results of the internal cell impedance are therefore inconclusive.

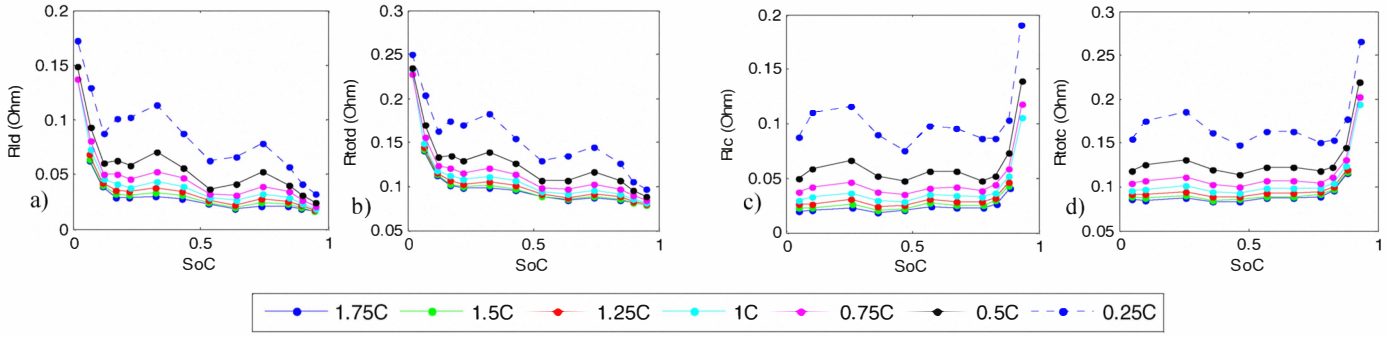

Fig. 1. a) R_{ld}, b) R_{totd}, c) R_{lc} and d) R_{totc} determined at different C-rates between 1.75C and 0.25C.

TABLE VI. IMPEDANCE PARAMETERS FOR C-RATE DEPENDENCY

g_{i1d}	6.993E-1	g_{i1c}	-4.124E-1
g_{i2d}	-6.919E-1	g_{i2c}	-1.082
g_{i3d}	2.902E-1	g_{i3c}	-8.730E-1

IV. SIMULATION

To validate the proposed practical equivalent circuit-based model, the voltage response resulting from the model simulation is compared to the measured voltage. The model is implemented in Simulink and can be directly connected the rest of an EV system model. In Fig. 11 the simulation results of the practical equivalent circuit-based model for discharging and charging at reference temperature is shown.

The voltage behaviour of the cell in Fig. 11 for both discharging and charging is accurately modelled. For discharging down to 10% SoC the simulation only has a maximum error of 11mV or 1% of the operating voltage range. But below 10% SoC the total cell impedance rises exponentially and the maximum error goes up to 10%. The inaccuracy is mainly due to the inaccurate fit of the long time transient parallel RC pair in the exponential region. A higher accuracy can be achieved if more parallel RC pairs are used in the model or if R_{ld} and C_{ld} are modelled with higher order polynomials; on the other hand, this would severely complicate the model while the inaccuracy in the linear region is very small. Furthermore, in EV applications battery cells will rarely operate in the region below 10% SoC, so the inaccuracy in this region is of very little importance.

For charging the same accuracy is observed. Up to 90% SoC the maximum error is 12mV or 1.1% of the operating voltage range. Above 90% SoC the maximum error rises to 6%. For charging the inaccuracy is also mainly caused by the exponential curve fit of the long time transient parallel RC pair. The accuracy can be improved in the same way as for discharing; however, the accuracy gained is small compared to the increased complexity. To extend the life of battery cells, some battery management systems are programmed to charge the cells up to 90% SoC. As the life time of battery cells are a very important factor in EV applications, it is expected that SoCs higher than 90% is prevented. Even if the cell is charged to 100%, the errors are acceptable small. Therefore the equivalent circuit-based model can sufficiently model the voltage behaviour in EV applications.

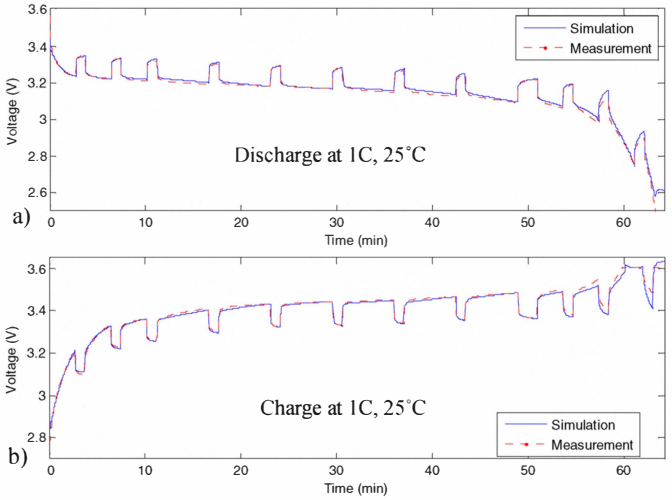

Fig. 11. Comparison between simulation and measurement for a) discharging and b) charging.

Modelling of the temperature and C-rate dependency is also validated in Fig. 12. For high temperatures the maximum voltage error for both discharging and charging is similar to the error found at reference temperature. However, at low temperatures the error becomes significantly large as shown in Fig. 12c and d for 0°C. The error has been determined to grow from 15°C. Using the equations for high temperature, at 15°C the maximum error is 20mV in the linear voltage range, going up to 80mV in the nonlinear range. Using the equations for low temperatures in the Appendix the low temperature behaviour of the cell can be modelled more accurately.

Simulations including C-rate dependency modelling show a maximum error of 14mV or 1.3% of the total voltage range for cells discharged with different C-rate. But if the C-rate dependency is neglected, the maximum error is doubled and a constant error is present in the voltage response, which becomes more profound at low C-rates. So depending on the required accuracy and operating conditions the temperature and C-rate dependency can be chosen to be taken into account.

The parameters are determined under a unidirectional current. It has therefore not been determined what the dynamics between switching between discharging and charging will be. The assumption is made that the impedance element equations for discharging is directly switched to charging when the current direction changes. Future works can include an investigation on the switching dynamics of the current from discharge to charge.

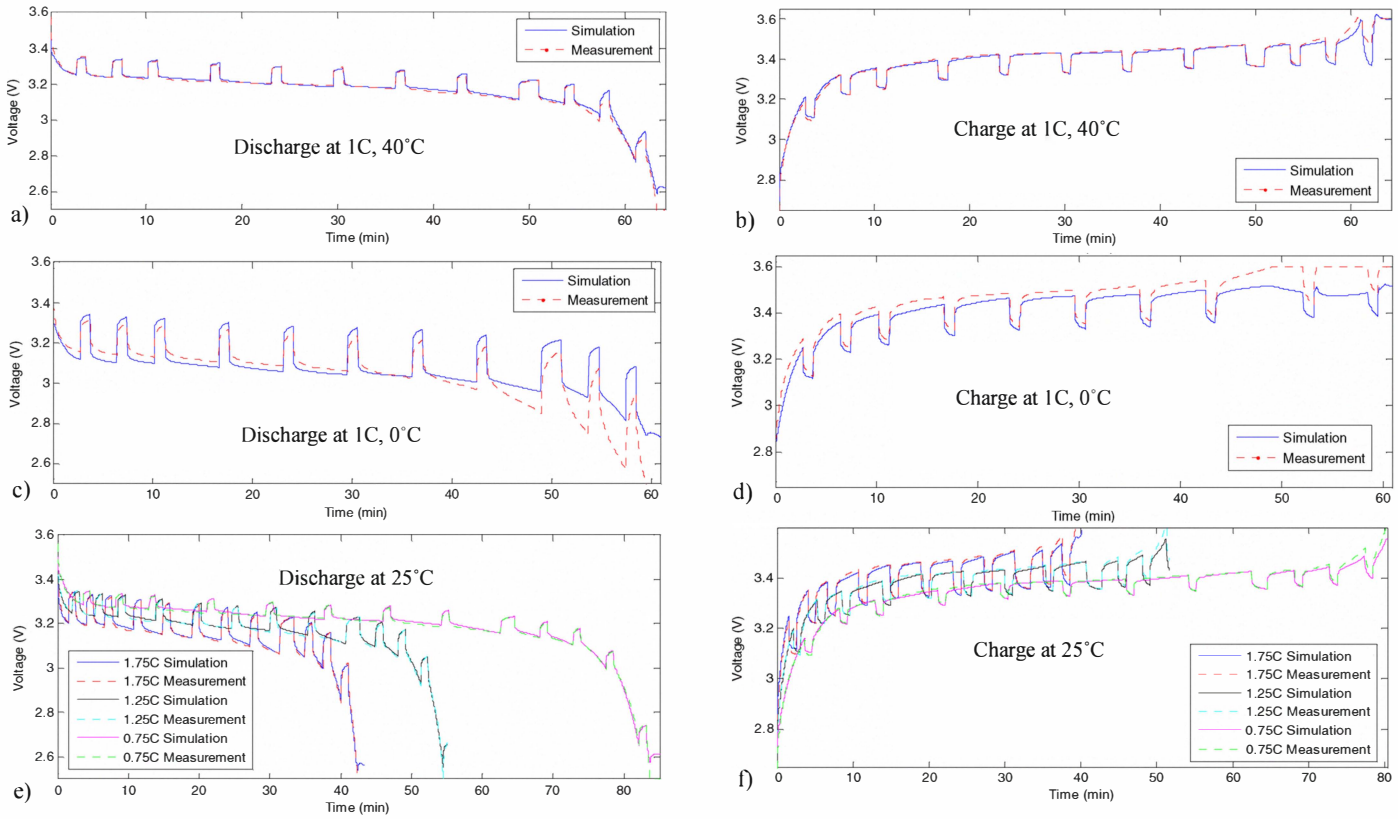

Fig. 2. Comparison between simulation and measurement for a) discharge at 40˚C 1C, b) charge. at 40˚C 1C, c) discharge at 0˚C 1C with high temperature model, d) charge at 0˚C 1C with high temperature model, e) discharge at 25˚C with different C-rates and f) charge at 25˚C with different C-rates.

V. CONCLUSION

A practical equivalent circuit-based model for EV applications is presented in this paper, which is capable of accurately modelling the behaviour of a $LiFePO_4$ cell under various operating conditions. Tradeoffs between complexity and accuracy of the model have been made based on practical situations in EV applications. The goal of the proposed model is to provide EV system designer with a tool to accurately simulate the behaviour of $LiFePO_4$ cells under possible operating conditions and optimise the battery operating range. From experiments equations have been extracted to describe the short term behaviour of the useable capacity and voltage response of the cell.

Between 90% and 10% SoC the model accurately represents the voltage response, with a maximum error of 12mV or 1.1% of the operating voltage range at reference temperature and 1C. However, at different temperatures and C-rates the maximum error triples compared to the reference conditions. To reduce the error empirical equations modelling the temperature and C-rate dependency of the cell have been proposed, which have a maximum error to 14mV. Ageing effects on the internal cell impedance have also been investigated, but were inconclusive. Depending on the required accuracy of the model and operating conditions of the cells, an EV system designer can choose the influences to be included in a system simulation.

ACKNOWLEDGMENT

This work was supported by High Tech Automotive Systems (HTAS) under project Databox.

APPENDIX

The empirical equations modelling the low temperature dependence of $LiFePO_4$ cells for discharge and charge are as follows with the parameters given in respectively Table VII and VIII.

$$R_{od,T_{low}}(SoC,T) = (b_{t1d}T^3 + b_{t2d}T^2 + b_{t3d}T + b_{t4d})SoC^4 + b_{2d}SoC^3 + b_{3d}SoC^2 + b_{4d}SoC + b_{t5d}e^{\frac{b_{t6d}}{T-b_{t7d}}} \quad (A1)$$

$$R_{sd,T_{low}}(SoC,T) = (c_{t1d}T^2 + c_{t2d}T + c_{t3d}) \cdot e^{-(c_{t4d}T^2 + c_{t5d}T + c_{t6d})SoC} + c_{3d} + c_{4d}SoC \quad (A2)$$

$$C_{sd,T_{low}}(SoC,T) = d_{1d}(SoC + (d_{t1d}T - d_{t2d}))^3 + d_{2d}(SoC + (d_{t1d}T - d_{t2d}))^2 + d_{4d} + (d_{t3d}T^2 + d_{t4d}T + d_{t5d})(SoC + (d_{t1d}T - d_{t2d})) \quad (A3)$$

$$R_{ld,T_{low}}(SoC,T,I) = g_{t1d}e^{\left(\frac{g_{t2d}}{T-g_{t3d}} - g_{2d}SoC\right)} + g_{t4d}e^{\frac{g_{t5d}}{T}} + g_{t6d}e^{\frac{g_{t7d}}{T}}SoC \quad (A4)$$

$$C_{ld,T_{low}}(SoC,T) = (h_{1d}SoC^4 + h_{2d}SoC^3 + h_{5d})e^{h_{t1d}T} + h_{3d}SoC^2e^{h_{t2d}T} + h_{4d}SoCe^{\frac{h_{t3d}}{T-h_{t4d}}}. \quad (A5)$$

$$R_{oc,T_{low}}(SoC,T) = (b_{1c}SoC^4 + b_{2c}SoC^3)(b_{t1c}T + b_{t2c}) + (b_{t3c}T^2 + b_{t4c}T + b_{t5c})SoC^2 + (b_{t6c}T^2 + b_{t7c}T + b_{t8c})SoC + b_{t9c}e^{\frac{b_{t10c}}{T-b_{t11c}}} \quad (A6)$$

$$R_{sc,T_{low}}(SoC,T) = c_{t1c}e^{c_{t2c}T+(c_{t3c}T+c_{t4c})SoC} + c_{t5c}T^2 + c_{t6c}T + c_{t7c} \quad \text{(A7)}$$

$$C_{sc,T_{low}}(SoC,T) = (d_{t1c}T^2 + d_{t2c}T + d_{t3c})SoC^4 + (d_{t4c}T^2 + d_{t5c}T + d_{t6c})SoC^3 + d_{t7c}e^{d_{t8c}T}SoC^2 + (d_{t9c}T^2 + d_{t10c}T + d_{t11c})SoC + d_{t12c}T + d_{t13c} \quad \text{(A8)}$$

$$R_{lc,T_{low}}(SoC,T) = g_{t1c} \cdot e^{g_{t2c}T - g_{2c}SoC} + g_{t3c}T^2 + g_{t4c}T + g_{t5c} + g_{4c}SoC \quad \text{(A9)}$$

$$C_{lc,T_{low}}(SoC,T) = (h_{t1c}SoC^5 + h_{t2c}SoC^4 + h_{t3c}SoC^3) \cdot e^{h_{t4c}T} + h_{t5c}e^{h_{t6c}T}SoC^2 + h_{t7c}e^{h_{t8c}}SoC + h_{t9c} \; . \quad \text{(A10)}$$

TABLE VII. LOW TEMPERATURE IMPEDANCE PARAMETERS DISCHARGE

b_{2d}	-2.819E-1	c_{4d}	-6.462E-3	d_{t2d}	4.068	g_{t7d}	4.202E3
b_{3d}	2.448E-1	c_{t1d}	1.923E-4	d_{t3d}	-6.807E-1	h_{1d}	-3.751E-11
b_{4d}	-9.630E-2	c_{t2d}	-1.166E-1	d_{t4d}	4.002E2	h_{2d}	6.764E-11
b_{t1d}	-5.930E-6	c_{t3d}	17.66	d_{t5d}	-5.769E4	h_{3d}	-2.219E-11
b_{t2d}	5.011E-3	c_{t4d}	1.098E-2	g_{2d}	20.00	h_{4d}	10.75
b_{t3d}	-1.411	c_{t5d}	-5.644	g_{t1d}	8.238E-3	h_{5d}	1.534E-13
b_{t4d}	1.325E2	c_{t6d}	7.299E2	g_{t2d}	1.805E2	h_{t1d}	1.220E-1
b_{t5d}	6.297E-2	d_{1d}	-1.173E3	g_{t3d}	2.321E2	h_{t2d}	1.241E-1
b_{t6d}	24.37	d_{2d}	8.278E2	g_{t4d}	1.589E-7	h_{t3d}	-4.492E2
b_{t7d}	2.363E2	d_{4d}	1.005E2	g_{t5d}	3.779E3	h_{t4d}	3.474E2
c_{3d}	1.827E-2	d_{t1d}	1.428E-2	g_{t6d}	-2.208E-8		

TABLE VIII. LOW TEMPERATURE IMPEDANCE PARAMETERS CHARGE

b_{1c}	2..192E-1	c_{t1c}	7.008E29	d_{t7c}	-3.688E-2	g_{t9c}	5.225
b_{2c}	-3.968E-1	c_{t2c}	-3.051E-1	d_{t8c}	4.261E-2	h_{t1c}	6.343E-6
b_{t1c}	-8.297E-2	c_{t3c}	2.782E-1	d_{t9c}	-1.199	h_{t2c}	-1.817E-5
b_{t2c}	24.82	c_{t4c}	-63.04	d_{t10c}	7.103E2	h_{t3c}	1.887E-5
b_{t3c}	2.136E-4	c_{t5c}	2.840E-6	d_{t11c}	-1.027E5	h_{t4c}	8.551E-2
b_{t4c}	-1.422E-1	c_{t6c}	-1.733E-3	d_{t12c}	8.493	h_{t5c}	-1.414E-5
b_{t5c}	23.48	c_{t7c}	2.786E-1	d_{t13c}	-1.902E3	h_{t6c}	8.381E-2
b_{t6c}	-1.795E-4	d_{t1c}	-11.23	g_{2c}	-32.23	h_{t7c}	1.057E-5
b_{t7c}	1.077E-1	d_{t2c}	5.941E3	g_{4c}	1.571E-2	h_{t8c}	7.897E-2
b_{t8c}	-16.20	d_{t3c}	-7.848E5	g_{t1c}	3.726E-8	h_{t9c}	6.962E2
b_{t9c}	4.968E-2	d_{t4c}	16.18	g_{t2c}	-4.951E-2		
b_{t10c}	28.78	d_{t5c}	-8.523E3	g_{t7c}	5.921E-5		
b_{t11c}	2.376E2	d_{t6c}	1.123E6	g_{t8c}	-3.507E-2		

REFERENCES

[1] R. Rao, S. Vrudhula, and D. N. Rakhmatov, "Battery modeling for energy-aware system design," *Computer*, vol. 36, no. 12, pp. 77–87, Dec. 2003.

[2] D. Rakhmatov, "Battery Voltage Modeling for Portable Systems," *ACM Trans. on Design Automation of Electronic Systems*, vol. 14, no. 2, 2009.

[3] M. Safari, M. Morcrette, A. Teyssot, and C. Delacourt, "Multimodal Physics-Based Aging Model for Life Prediction of Li-Ion Batteries," *J. Electrochem. Soc.*, vol. 156, no. 3, pp. A145-A153, 2009.

[4] W. B. Gu and C. Y. Wang, "Thermal and electrochemical coupled modeling of a lithium-ion cell in lithium batteries," in *Proc. ECS*, 2000, pp.748–762.

[5] P. Rong and M. Pedram, "An analytical model for predicting the remaining battery capacity of lithium-ion batteries," *IEEE Trans.VLSI Systems*, vol.14, no.5, pp.441-451, May 2006.

[6] S. Santhanagopalan, Q. Zhang, K. Kumaresan, and R. E. White, "Parameter Estimation and Life Modeling of Lithium-Ion Cells," *J. Electrochem. Soc.*, vol. 155, no. 4, pp. A345-A353, 2008.

[7] M. W. Verbrugge and R. S. Conell, "Electrochemical and Thermal Characterization of Battery Modules Commensurate with Electric Vehicle Integration," *J. Electrochem. Soc.*, Vol. 149, no. 1, pp. A45-A53, 2002.

[8] B. Y. Liaw, G. Nagasubramanian, R. G. Jungst, and D. H. Doughty, "Modeling of lithium ion cells—A simple equivalent-circuit model approach," *Solid State Ionics,* vol. 175, no. 1-4, pp. 835-839, 2004.

[9] S. S. Zhang, K. Xu, and T. R. Jow, "Electrochemical impedance study on the low temperature of Li-ion batteries," *Electrochim. Acta*, vol. 49, no. 7, pp. 1057-1061, 2004.

[10] P. Suresh, A. K. Shukla, and N. Munichandraiah, "Temperature dependence studies of a.c. impedance of lithium-ion cells," *J. Applied Electrochem.*, vol. 32, no. 3, pp. 267-273, 2002.

[11] Y. Hu, S. Yurkovich, Y. Guezennec, and B.J. Yurkovich, "Electro-thermal battery model identification for automotive applications," *J. Power Sources*, vol. 196, no. 1, pp. 449-457, 2011.

[12] L. Gao, S. Liu, and R. A. Dougal, "Dynamic lithium-ion battery model for system simulation," *Components and Packaging Technologies, IEEE Trans. on*, vol.25, no.3, pp. 495- 505, 2002.

[13] P. Kumar and P. Bauer, "Parameter Extraction of Battery Models Using Multiobjective Optimization Genetic Algorithms," *EPE/PEMC, 2010 14th International*, pp. T9-106-T9-110, 2010.

[14] Y. Hu, S. Yurkovich, Y. Guezennec, and B. J. Yurkovich, "A technique for dynamic battery model identification in automotive applications using linear parameter varying structures," *Control Eng. Practice*, vol. 17, no. 10, pp. 1190-1201, 2009.

[15] M. Chen and G.A. Rincón-Mora, "Accurate Electrical Battery Model Capable of Predicting Runtime and *I-V* Performance," *IEEE Trans. on Energy Conv.,* vol. 21, no. 2, pp. 504-511, 2006.

[16] J. Zhang, S. Ci, H. Sharif, and M. Alahmad, "An Enhanced Circuit-Based Model for Single-Cell Battery," *APEC*, pp. 672-675, 2010.

[17] O. Erdinc, B. Vural, and M. Uzunoglu, "A dynamic lithium-ion battery model considering the effects of temperature and capacity fading," *Int. Conf. on Clean Electrical Power*, pp.383-386, 2009.

[18] H. L. Chan and D. Sutanto, "A new battery model for use with battery energy storage systems and electric vehicles power systems," *IEEE Power Eng. Soc. Winter Meeting*, vol.1, pp.470-475, 2000.

[19] S. Mischie and D. Stoiciu, "A new and improved model of a lead acid battery" *J. FACTA UNIVERSITATIS*, vol. 20, no. 2, pp. 187–202, 2007.

[20] R.C. Kroeze and P.T. Krein, "Electrical battery model for use in dynamic electric vehicle simulations," *PESC,* pp.1336-1342, 2008.

[21] M. Dubarry, V. Svoboda, R. Hwu, and B. Y. Liaw, "Capacity loss in rechargeable lithium cells during cycle life testing: The importance of determining state-of-charge, " *J. Power Sources*, vol. 174, no. 2, pp. 1121-1125, 2007.

[22] E. Kuhn, C. Forgez, P. Lagonotte and G. Friedrich, "Modelling Ni-mH battery using Cauer and Foster structures", *J. Power Sources*, vol.158, no. 2, pp. 1490-1497, 2006.

[23] L. Alexander, S. Mani, and D. Carmen, "Development of battery packs for space applications," *NASA Aerospace Battery workshop*, 2007.

[24] M. A. Roscher and D. U. Sauer, "Dynamic electric behavior and open-circuit-voltage modeling of LiFePO4-based lithium ion secondary batteries", *J. Power Sources*, vol. 196, no. 1, pp. 331-336, 2011.

[25] F. Baronti, G. Fantechi, E. Leonardi, R. Roncella, and R. Saletti, "Enhanced model for Lithium-Polymer cells including temperature effects," *IECON 2010*, pp. 2329-2333, 2010.

[26] S. Abu-Sharkh and D. Doerffel, "Rapid test and non-linear model characterisation of solid-state lithium-ion batteries", *J. Power Sources*, vol. 130, no. 1-2, pp. 266-274, 2004.

[27] B. Schweighofer, K. M. Raab, and G. Brasseur, "Modeling of high power automotive batteries by the use of an automated test system," *IEEE Trans.Instrum. Meas.*, vol. 52, no. 4, pp. 1087–1091, 2003.